Supplemental Information for:

Gal8 Visualization of Endosome Disruption Predicts Carrier-mediated Biologic Drug Intracellular Bioavailability

Kameron V. Kilchrist, Somtochukwu C. Dimobi, Meredith A. Jackson, Brian C. Evans, Thomas A. Werfel, Eric A. Dailing, Sean K. Bedingfield, Isom B. Kelly, Craig L. Duvall

Department of Biomedical Engineering, Vanderbilt University, PMB 351634, Nashville, Tennessee 37235, United States

Corresponding author: craig.duvall@vanderbilt.edu

Contents

S1: PEG-b-(DMAEMA-co-BMA) Polymer Synthesis Scheme

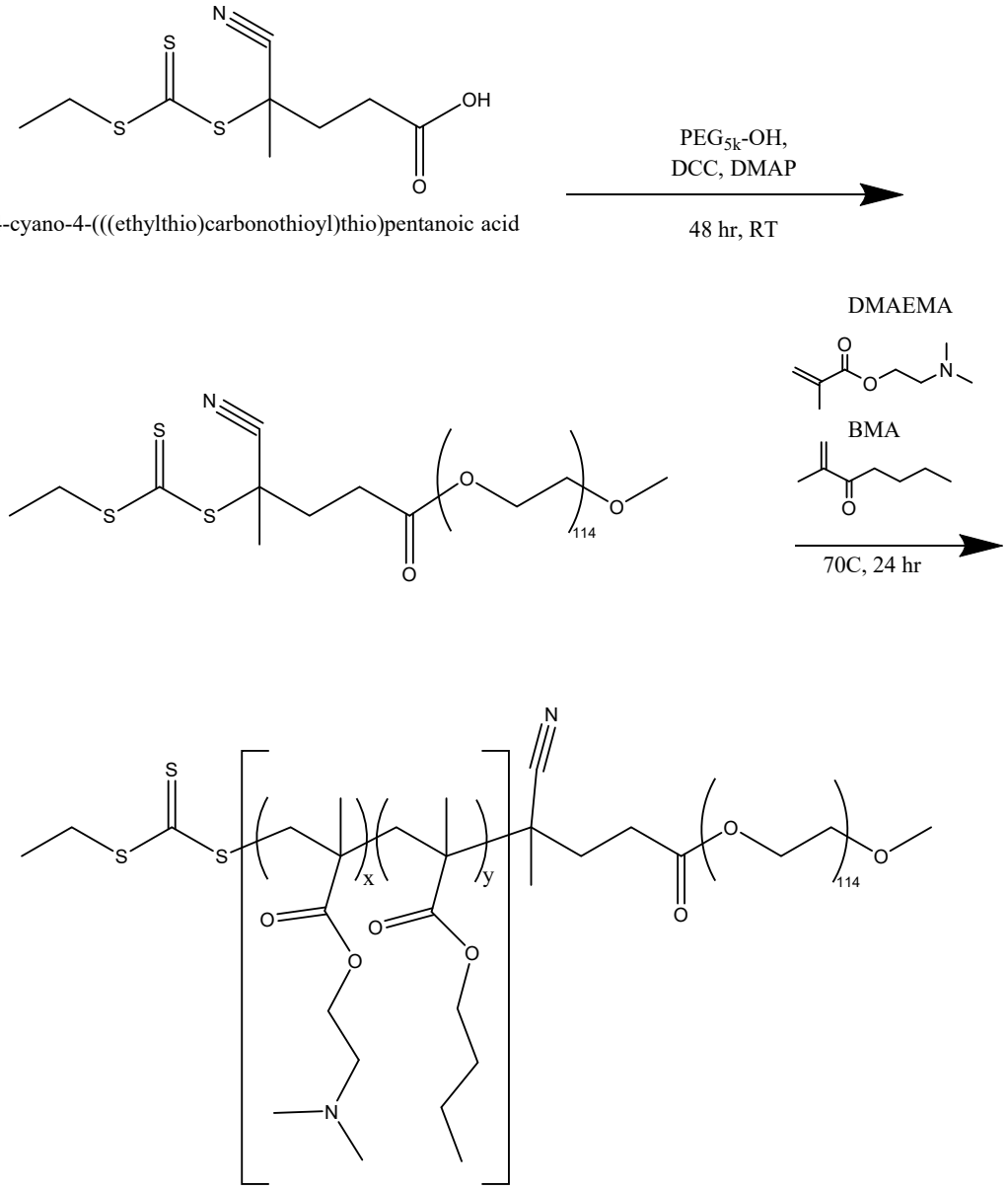

Reaction scheme 1. Synthesis of PEG macro CTA for RAFT synthesis.

S2: 50B Molecular Weight Library, Viability Data

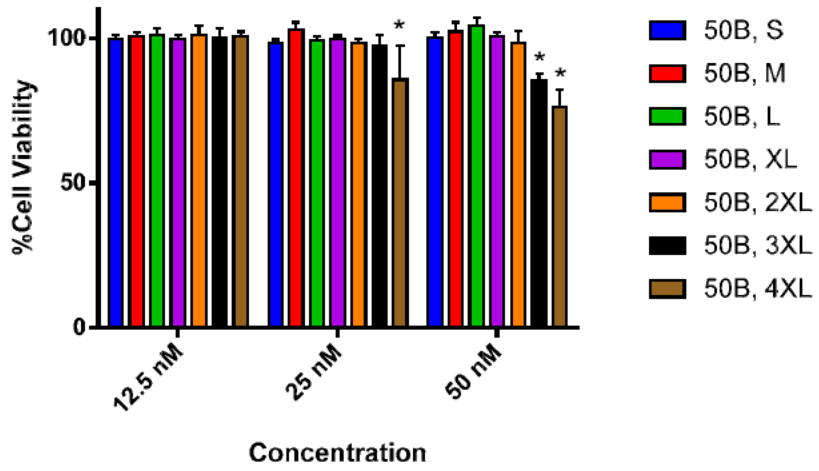

Figure S2: Formulations nontoxic, except modest toxicity for largest polymers and highest doses. Cells treated at indicated doses and assayed according to CellTiterGlo instructions.

S3: Gal8 Image Processing Pipeline

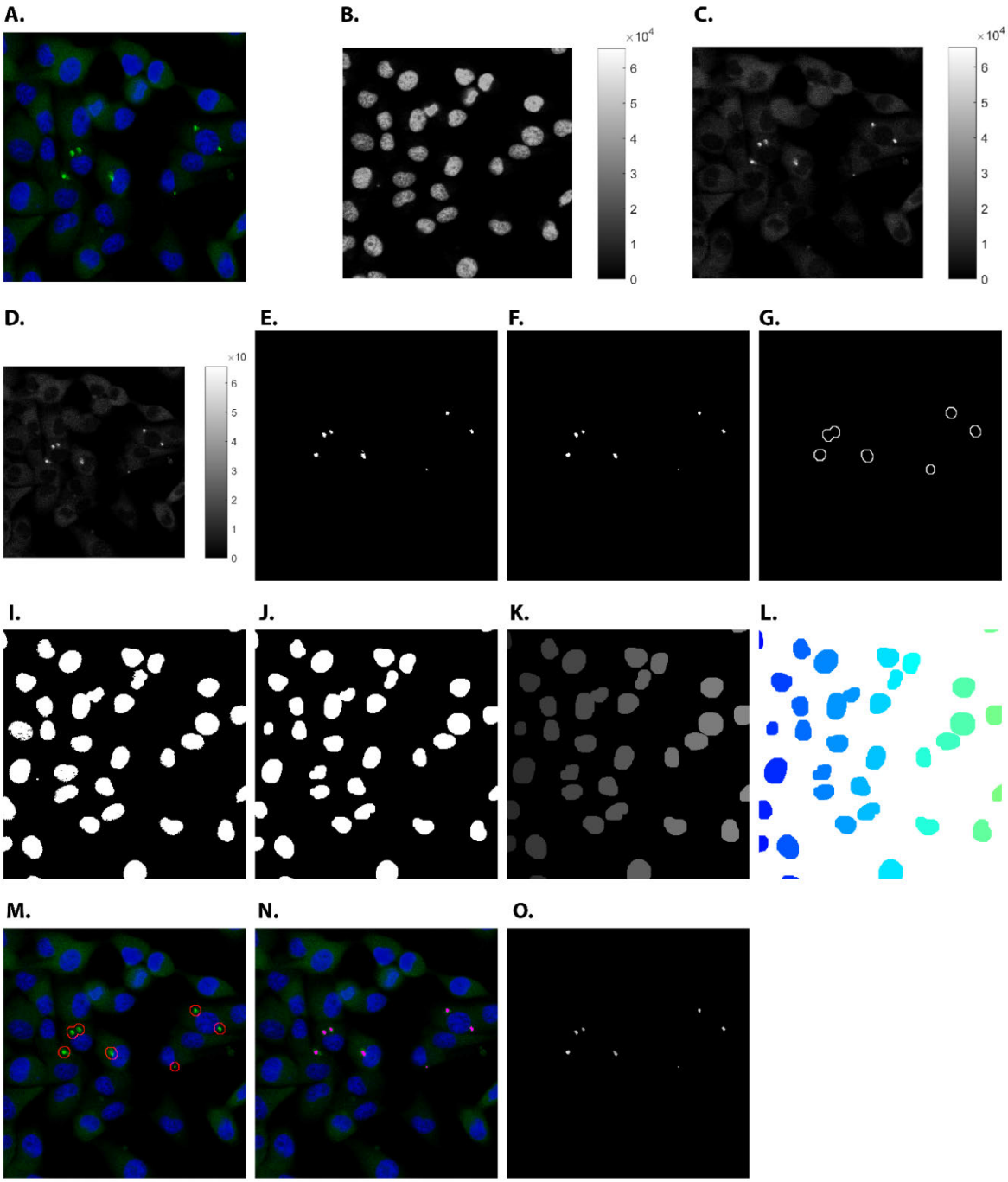

A: Original composite micrograph
B: Nuclear stain channel
C: Gal8 channel
D: Gal8 following tophat filter of *C*
E: Simple threshold of *D* to identify positive pixels
F: Morphological opening of *E*
G: Annotation layer generated using *E*, denoting positive spots
I: Simple threshold of B
J: Morphological opening of *I* to separate proximal nuclei
K: Watershed transform of *J*
L: Rainbow colormap applied to *K*
M: Exported composite, with annotations (red)
N: Exported composite, false color "positive spots" (red)
O: Binary mask of "positive spots"

S4: Full size image of Figure 5B1, showing AuNP treated control

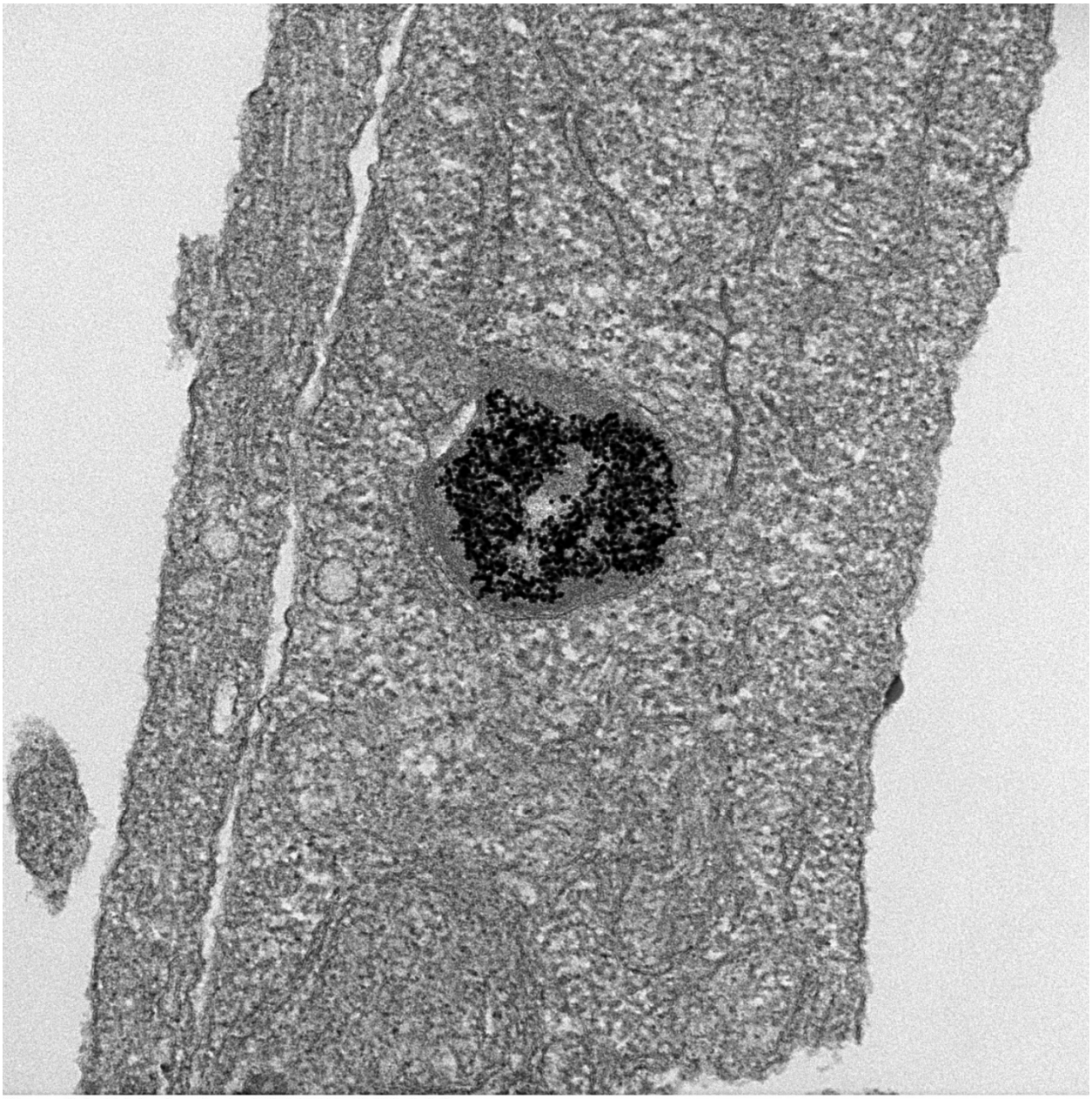

S5: Full size image of Figure 5B2, showing AuNP/50B-S treated cells

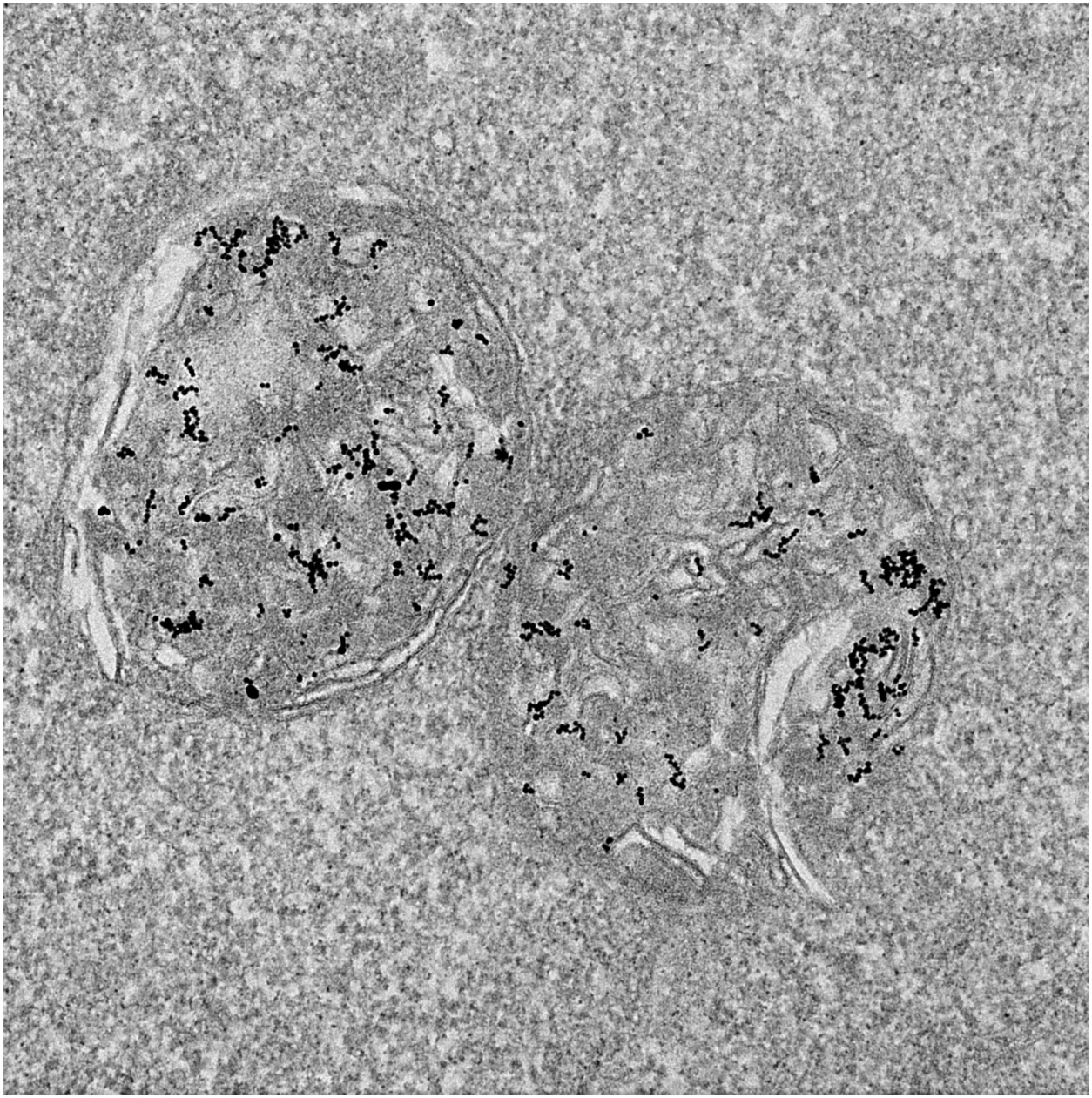

S6: Full size image of Figure 5B3, showing AuNP/50B-L treated cells

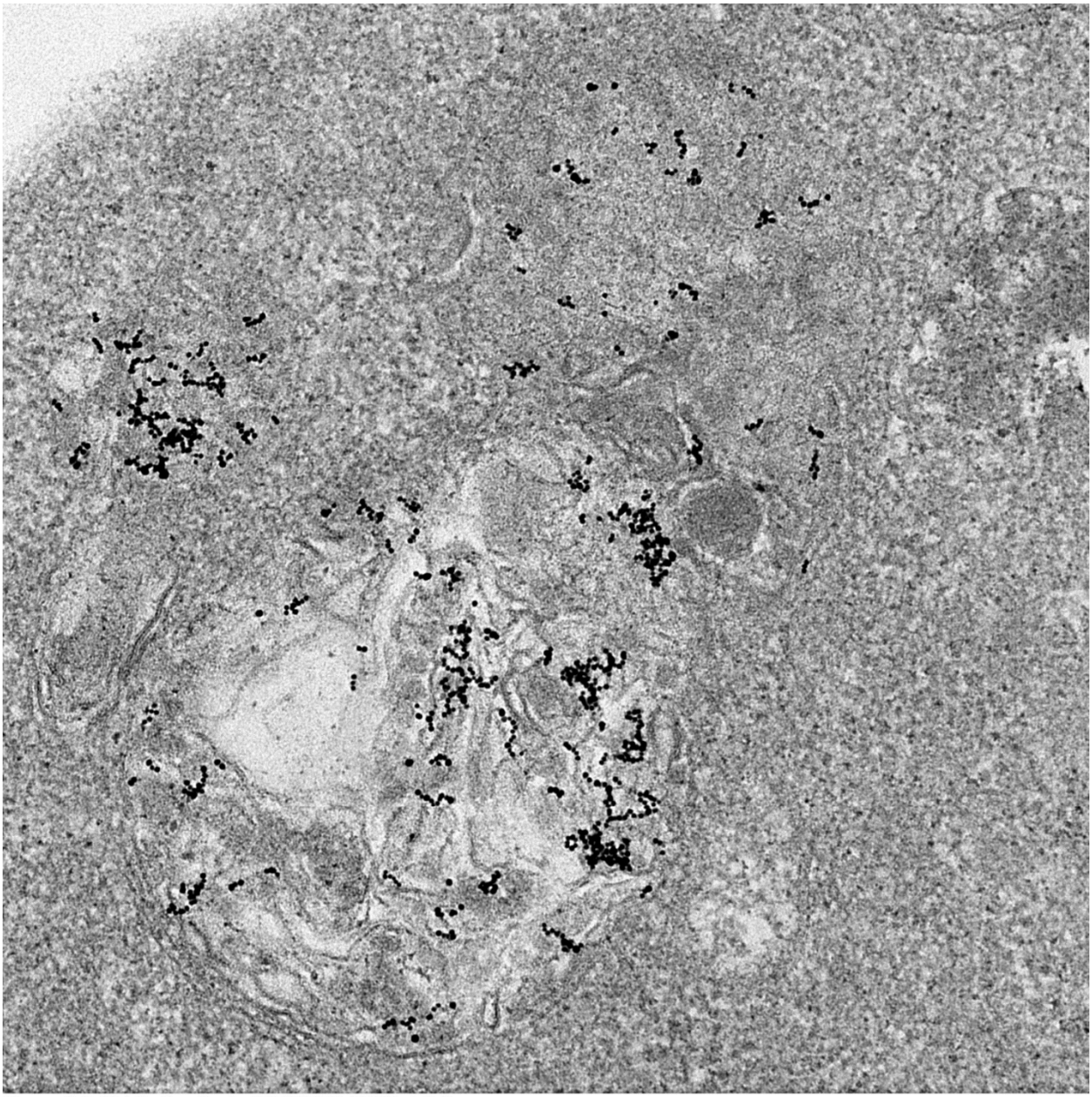

S7: Full size image of Figure 5B4, showing AuNP/50B-4XL treated cells

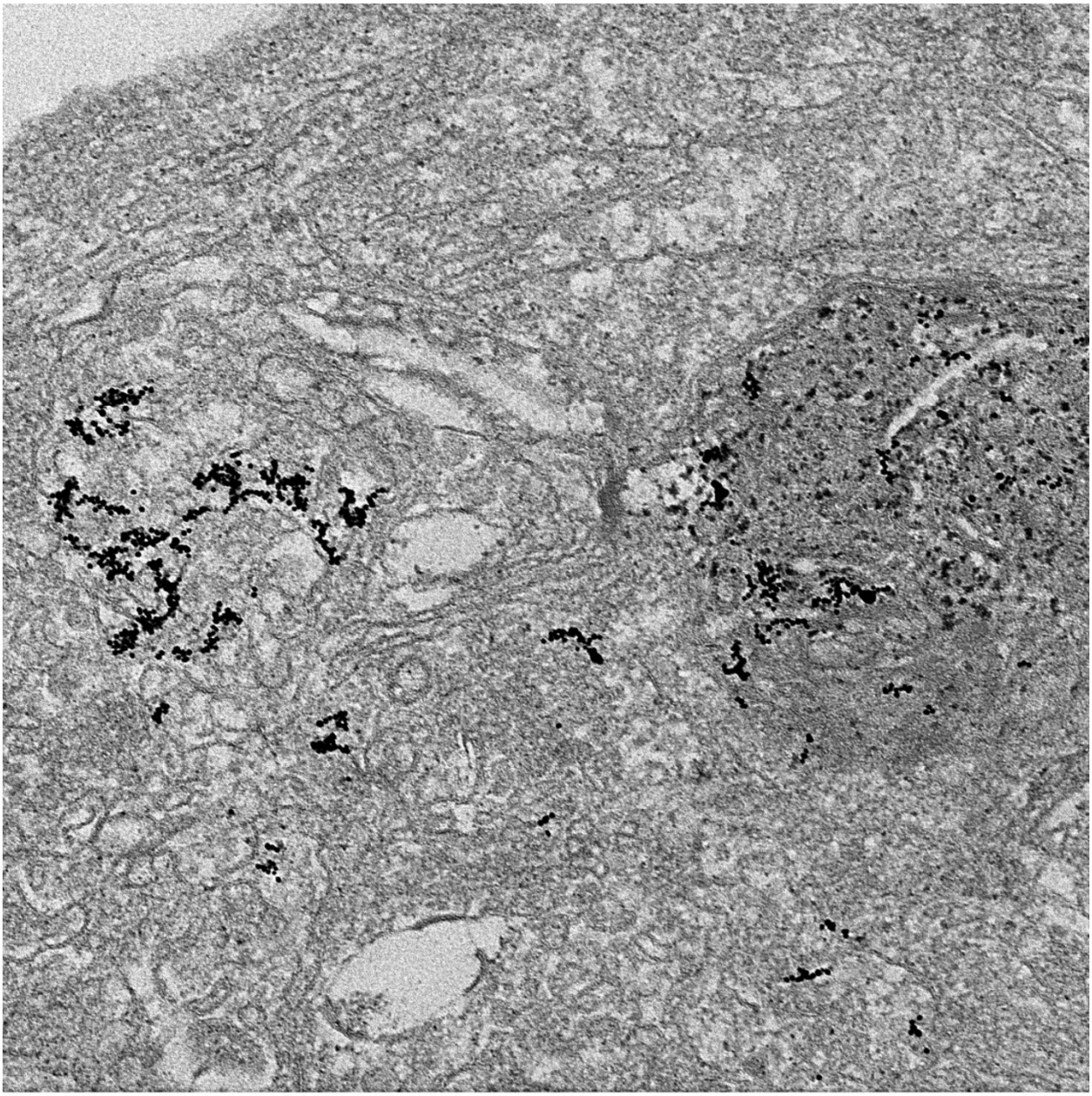

S8: Cellular uptake of siRNA in 50B Molecular Weight Library

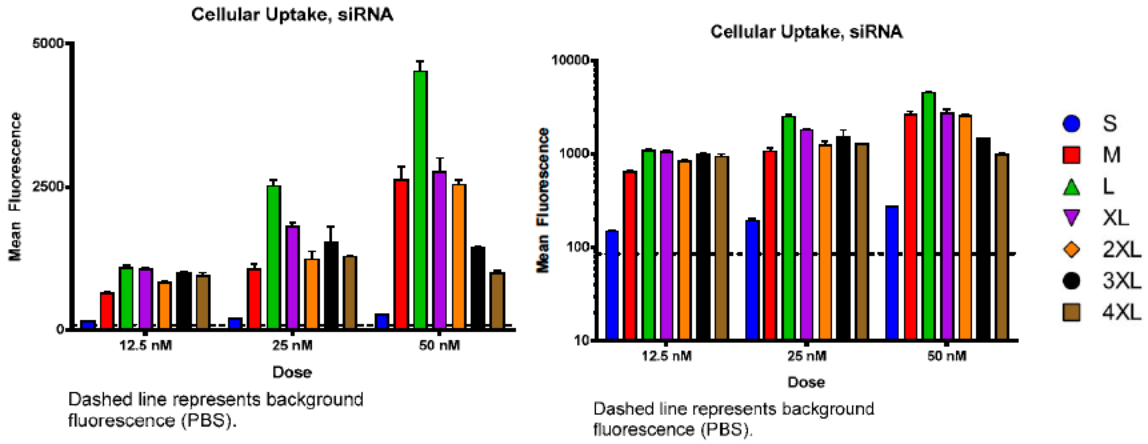

Mean fluorescence intensity was measured using flow cytometry at 12.5, 25, and 50 nM doses of Alexa-488 dsDNA in polyplexes and plotted on both linear (left) and log (right) scales. Cells treated with buffer produced fluorescence represented by the dotted line.

S9: Polymer molecular weight correlates with luciferase knockdown in 50B MW library

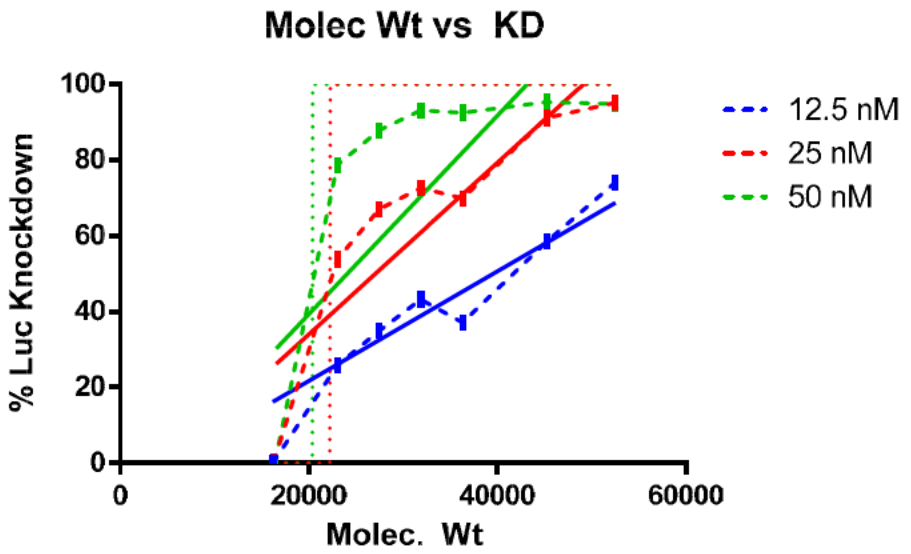

Polymer molecular weights correlate strongly with gene knockdown data at 12.5 nM (blue circles), 25 nM (red squares), and 50 nM (green triangles). These correlations are statistically significant by Spearman's method. Solid line indicates simple linear regression. Dashed line connects adjacent datapoints. Dotted lines represent the sigmoidal best fit, constrained with plateaus at 0% and 100%.

All three doses produce ~0 knockdown at the 16300 g/mol MW. Likewise, 50 and 25 nM doses overlap at the largest MW, 52500 g/mol.

Due to non-linear effects which become increasingly apparent at high doses (maximal knockdown of 100%, ~0% knockdown for all molecular weights below ~16500 g/mol), the 95% confidence interval for the slope of the linear regression for 50 nM does not exclude 0 slope, representing saturation of the assay as mentioned in the text.

A sigmoidal curve is likely the most appropriate model for such a system with constraints at both the low (=0%) and high (=100%) end, but the best fit to this model does not converge for the 12.5 nM dose, while for the 25 and 50 nM doses it produces an ambiguous response. Still, such a fit suggests a Log EC50 of 22237 and 20395 MW for 25 and 50 nM, respectively, suggesting polymers below these molecular weights may not be useful for gene knockdown. There may be interesting nonlinear polymer effects in this range of molecular weights.

Statistics for Fig S9:

	KD, 12.5 nM		KD, 25 nM		KD, 50 nM	
	r	*p*	*r*	*p*	*r*	*p*
Molec Weight	0.96	0.003	0.96	0.003	0.93	0.007

S10: Gal8 Recruitment Correlates to Gene Knockdown in Immortalized Rat Smooth Muscle Cells (A7r5)

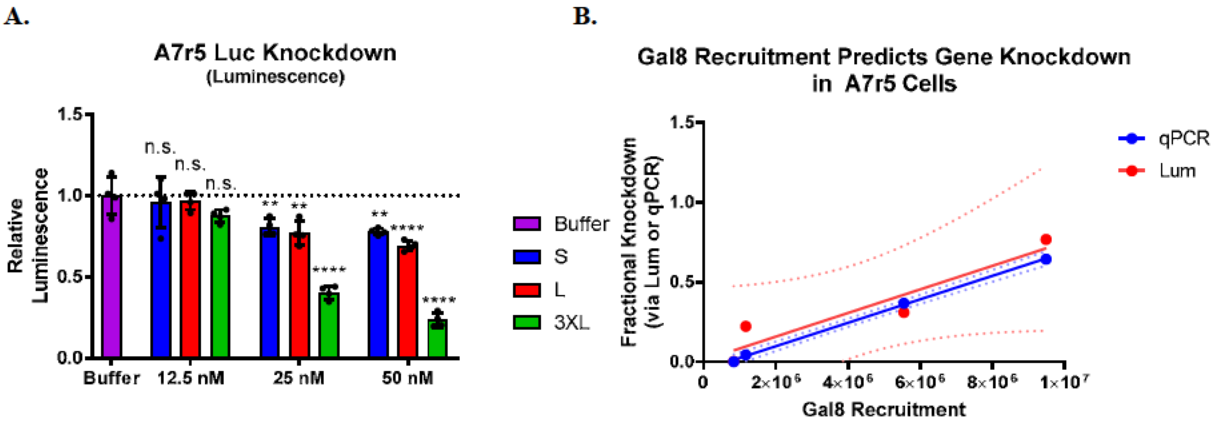

(A): A7r5 cells were treated with indicated concentrations of scrambled and siLuc sequences of siRNA. After 24 h of treatment, media was exchanged and luminescence was measured. The symbols *, **, ***, and **** represent $p < 0.05$, 0.01, 0.001, and 0.0001 respectively.

(B): Gal8 recruitment (From Figure 6F) was plotted on the x-axis against PHD2 levels (from Figure 6E) and luminescence levels (from Figure S10A) on the y-axis, and subjected to linear regression (solid lines, ± 95% confidence interval are dotted lines) and correlation analysis by Pearson's method. The correlation of the Gal8 to qPCR correlation was $r = 0.9995$, $p = 0.0005$ and the correlation of the Gal8 to knockdown by luminescence was $r = 0.94$, $p = 0.06$. This is summarized in the table below.

Statistical Summary, Figure S10B		
Gal8 correlation to:	**qPCR**	**Luminescence**
r	0.9995	0.94
R^2	0.999	0.8836
P (two-tailed)	0.0005	0.06

S11: Spatial heterogeneity within Tumor Gal8 recruitment

A.

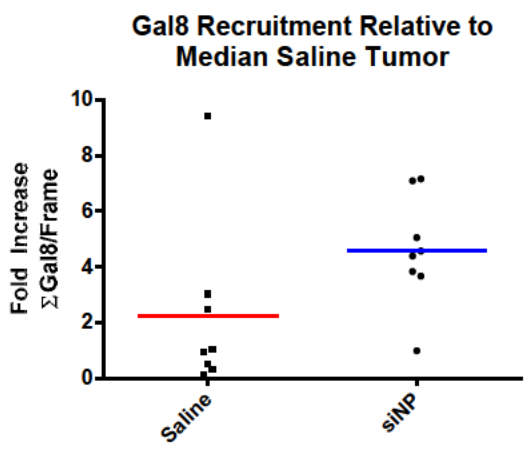

B.

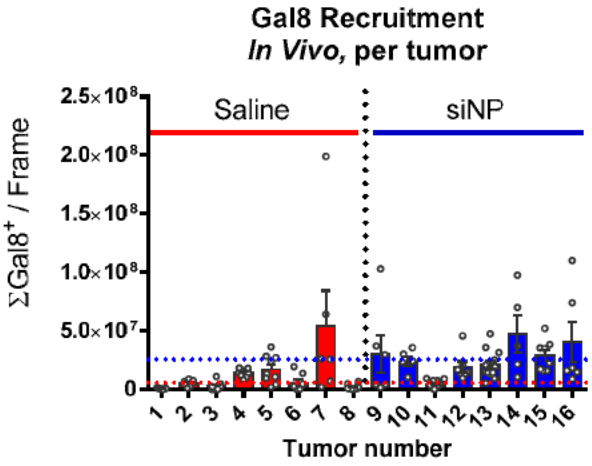

Tumors exhibited varying degrees of endosomal disruption.

A) An alternate plot of figure 7A, showing relative Gal8 recruitment relative to the median saline treated tumor's Gal8 recruitment measurement.

B) Some saline treated tumors (left) had Gal8 recruitment, and some locations within tumors of siNP treated mice (right) did not show Gal8 recruitment. Overall, siNP tumors were found to contain significantly more Gal8 recruitment. Lower, red ($0.57 * 10^7$) and upper, blue ($2.57 * 10^7$) dotted lines indicates the median tumor's average Gal8 recruitment *per* frame for saline and siNP treated mice, respectively. The median tumor's average Gal8 recruitment was 4.5 fold higher in siNP treated mice.

S12: Stably integrated genetic constructs do not substantially impact MDA-MB-231 siNP uptake.

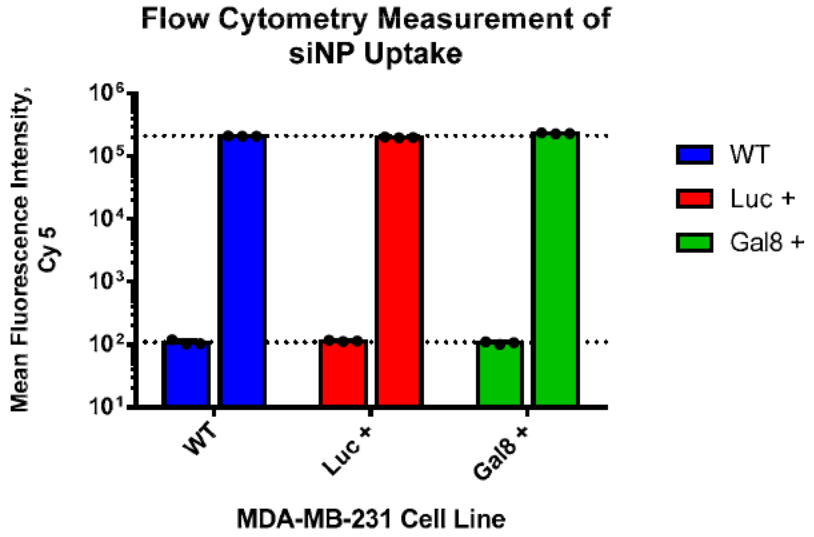

To assess whether stably integrated genetic constructs altered cellular uptake of 50B particle uptake, MDA-MB-231 cells (wild type, Luc+, and Gal8+) were treated with 50 nM Cy5 labeled siRNA loaded into 50B-L polyplexes for 24 hr then subjected to flow cytometric analysis of cellular fluorescence *per* methods in the main text.

Bar height represents mean fluorescence intensity of Cy5 channel; error bar represents standard deviation. Most error bars are too small to visualize on plot. Dashed lines represent the mean Cy5 fluorescence for siNP treatment (upper) and mean basal fluorescence (lower) of WT, Luc +, and Gal8 + cells.

Two-way analysis of variance (ANOVA) reveal that siNP treatment, genetic construct, and interaction thereof are statistically significant ($p < 10^{-4}$) contributors to dataset variance. siNP treatment contributes the overwhelming majority (99.2%) of dataset variation, while genetic construct and interaction with siNP treatment contributes 0.39% of variation each.

As over 99% of the total variance is explained by siNP treatment, we are satisfied that genetic constructs do not meaningfully alter siNP uptake relative to wild type MDA-MB-231 cells.

Supplemental Table 1: Correlation and statistics, Δ Hemolysis *versus* Knockdown

	KD, 12.5 nM		KD, 25 nM		KD, 50 nM	
	r	*p*	*r*	*p*	*r*	*p*
Hemolysis, pH 7.4	0.96	0.003	0.96	0.003	0.93	0.01
Hemolysis, pH 6.8	0.54	0.23	0.54	0.24	0.43	0.35
Hemolysis, pH 6.2	-0.36	0.44	-0.36	0.44	-0.46	0.30
Δ Hemolysis, pH 7.4-6.8	0.04	0.96	0.04	0.96	0.00	>0.99

Technical Note 1: Lines of best fit for correlation data

As with many biological phenomena, the underlying system is nonlinear. It appears that, with this system, Gal8 recruitment can continue to increase, even after enough siRNA has already been released to saturate/maximized measurable gene knockdown.

Because the siRNA knockdown saturates before Gal8 recruitment, we chose a hyperbolic fit to account for the asymptote of 100% gene knockdown in MDA-MB-231 cells. However, to further understand these data, we performed additional analysis. A linear fit constrained to pass through the origin provides an r^2=0.2701 for the whole dataset, but excluding the seven highest formulation-dose combinations that induced nearly saturating knockdown (>80%), the r^2 of the linear fit increases to r^2=0.8019. We see that these high values contribute to the deviation from a linear model. Even in that case of excluding the highest 7 values of knockdown (which are also the highest 7 values of Gal8 recruitment), a hyperbolic fit is still more appropriate ($p<0.0001$); with the linear fit resulting in 3.2-fold higher error (sum of squared residuals). For the full dataset (including the 7 highest points), a linear fit contains 15.7-fold more error (sum of squared residuals) than the hyperbolic fit. We therefore concluded the hyperbolic fit is the appropriate fit for this dataset, with both strong biological and statistical rationale.

For the A7r5 dataset (Figure 6G), the rationale for a linear fit was twofold. One, the dataset contains fewer datapoints, resulting from the subset of polymers and doses tested (because in this cell line, knockdown was measured using qPCR), necessitating a simpler fit to avoid overfitting. Further, insufficient information is available to assess whether saturating effects were occurring in this cell line at this dose. These observed differences may be due to myriad biological differences (e.g., differences in uptake, intracellular trafficking, endosomal integrity) between human metastatic breast cancer cells (MDA-MB-231) and rat smooth muscle cells (A7r5). Thus, without substantial rationale to support a more complicated model, we chose a linear best fit. In both the case of Figure 6A and 6G, the lines of best fit are to guide the reader to see trends we believe are present in the data, but were calculated independently of correlation and statistics.

Technical Note 2: Microscopy requirements

Gal8 recruitment induces bright puncta against a relatively dim background, which are then identified algorithmically. The pixel intensities within these puncta are then integrated (summed). In exploring the data generated by this technique, we found this quantification method to be the most robust and generalizable.

We have found this method to require a relatively low power objective (herein, a 20x) because it is not necessary to resolve two nearby disrupted endosomes from each other, so long as the total disruption is still quantified. (Higher power objectives may be needed for single endosome tracking studies, small cells, or time course experiments tracking a small number of cells.) Two, because our method integrates identified spots of high intensity, it minimizes the contribution of "false positives," *e.g.*, areas that are identified algorithmically as Gal8 positive but do not contain disrupted endosomes or particularly bright pixels, as encountered in spots of true Gal8 recruitment. These false positives spots contribute only a small amount to the sum of Gal8 intensity within Gal8+ spots, but would contribute a proportionately larger error in methods tracking the area fraction of Gal8+ or % Gal8+ cells.

The use of the 20x objective and this robust algorithm also affords another advantage. Our use of the 20× objective was critical to obtaining large fields of view, but also provided a thick optical slice in which the majority of the cytoplasm was in focus throughout the entire frame. In our hands, the low power 20x objective was far easier to focus than higher power 40x or 60x objectives, and still provided adequate resolution to resolve endosomes algorithmically when combined with a 2048 x 2048 pixel acquisition image. These large fields of view contained more cells (~200) which further increased the robustness of the system when combined with high quality, high-flatness glass coverslip bottom plates.

When combined with a nuclear stain, this approach also allowed "blinded" focusing of the microscope system on the MDA-MB-231 cell. Between this thick optical slice, automated focusing, and the robust quantification algorithm, we were able to ensure objective data acquisition without user bias.

Implementing this method in other imaging systems may require the use of an autofocus algorithm, for which the nuclear channel would be well suited. This method does require an adequate resolution camera, adequate stage flatness, software-controlled stage and acquisition, *etc*. Each imaging system manufacturer has their own preferred implementation of focus assisting, usually based on some combination of hardware and software. However, in our hands, imaging based autofocus algorithms increased image acquisition time unacceptably and did not improve data quality.

Indeed, before executing this assay on a new optical system, pilot experiments should be conducted to ensure consistent and reproducible imaging and ensuring that the Gal8 signal remains within the focal plane. Appropriate method controls should be routinely employed when developing the method in house, especially to control for the potential effects of wash buffers, temperature and humidity changes, and other environmental factors that may affect endosomal integrity due to user manipulation of the cells.